Journal of Materials Chemistry C

PAPER

Cite this: J. Mater. Chem. C, 2016, 4, 1900

Lanthanide metal–organic frameworks assembled from a fluorene-based ligand: selective sensing of Pb^{2+} and Fe^{3+} ions†

Liang Li,[a] Qiang Chen,[a] Zhigang Niu,[b] Xinhui Zhou,*[a] Tao Yang[a] and Wei Huang*[ac]

Received 19th December 2015,
Accepted 3rd February 2016

DOI: 10.1039/c5tc04320d

www.rsc.org/MaterialsC

Fast and selective detection of heavy metal ions in the aqueous phase plays a key role in meeting human health and environmental concerns. Herein we report a series of fluorene-based lanthanide metal–organic frameworks ($[Ln_2(FDC)_3DMA(H_2O)_3]\cdot DMA\cdot 4.5H_2O$, Ln = Sm (**1**), Eu (**2**), Gd (**3**) and Tb (**4**), H_2FDC = 9,9-dimethyl-2,7-fluorenedicarboxylic acid, DMA = dimethylacetamide). Single crystal X-ray diffraction reveals that **1–4** are isostructural and display a 3D neutral framework. **2** exhibits intense characteristic red emission of Eu^{3+} ions in the solid state and high selectivity for Pb^{2+} and Fe^{3+} ions through fluorescence enhancement and the quenching effect in aqueous solutions, respectively. Interestingly, the fluorescence intensity of **2** shows a good linear relationship with Pb^{2+} concentration in the range of 0.02–0.1 mM. Furthermore, the dynamic and static quenching constants are calculated to be 320 M^{-1} and 10 680 M^{-1} by the fluorescence lifetime and titration experiments in low concentration of Fe^{3+}. In addition, **4** exhibits different fluorescence response behaviors in the presence of Sm^{3+} or Eu^{3+} in aqueous solution.

Introduction

Metal–organic frameworks (MOFs) have received great attention in the past fifteen years due to their interesting structures of various network topologies and tunable pore size, fascinating properties of breathing behavior, high surface area, and the availability of inner surface modification, and potential applications in gas separation, energy transformation, drug delivery, sensing, and heterogeneous catalysis.[1–5] The rich variety of linkers and metal centers has promoted the rapid development of luminescent MOFs. Taking advantage of the tunable luminescence and porous structure of some luminescent MOFs, a mountain of important progress has been made in the application of luminescent MOFs for sensing explosives, oxygen, small molecules and temperature. For example, Li's group has reported a Zn-based luminescent MOF which shows high sensitivity to RDX (1,3,5-trinitroperhydro-1,3,5-triazine) and ketone vapors.[6] Qian's group has reported a luminescent MOF film, the MIL-100(In) ⊃ Tb^{3+} film, which shows high oxygen sensitivity and fast response/recovery speed.[7] Dinca's group has reported Zn_2(TCPE) (TCPE = tetrakis(4-carboxyphenyl)ethylene) and Mg(H_2DHBDC) (H_2DHBDC^{2-} = 2,5-dihydroxybenzene-1,4-dicarboxylate) MOFs, both exhibiting interesting sensitivity to ammonia at 100 °C.[8] Chen and Qian synthesized a perylene doped Eu-MOF acting as a luminescent thermometer in the range of 20–80 °C.[9] Very recently, a lot of studies on luminescent MOFs for sensing heavy metal ions such as Fe^{3+} and Cu^{2+} ions have been developed on the basis of interactions between metal ions and Lewis base sites (N or O) within the ligands and energy or electron transfer from the ligand to metal ions.[10–18] Among the heavy metals, Pb^{2+} is often encountered in the environment and continues to be one of the most hazardous. A wide variety of diseases such as digestive, reproductive, neurological, and developmental disorders have been attributed to the excessive Pb^{2+} concentration in the body. Hence, selective sensing of Pb^{2+} seems to be very important. However, selective sensing of Pb^{2+} and Fe^{3+} through fluorescence enhancement and quenching in a luminescent lanthanide MOF has never been explored.

As a continuation of our work on functional luminescent MOF development, we herein report the synthesis of a series of lanthanide MOFs, namely $[Ln_2(FDC)_3DMA(H_2O)_3]\cdot DMA\cdot 4.5H_2O$, [Ln = Sm (**1**), Eu (**2**), Gd (**3**) and Tb (**4**), H_2FDC = 9,9-dimethyl-2,7-fluorenedicarboxylic acid, DMA = dimethylacetamide], and the

[a] Key Laboratory for Organic Electronics and Information Displays & Institute of Advanced Materials, National Jiangsu Syngerstic Innovation Center for Advanced Materials (SICAM), Nanjing University of Posts & Telecommunications, Nanjing, 210023, China. E-mail: iamxhzhou@njupt.edu.cn
[b] College of Chemistry and Chemical Engineering, Hainan Normal University, Haikou 571158, China
[c] Key Laboratory of Flexible Electronics (KLOFE) & Institute of Advanced Materials (IAM), Jiangsu National Synergetic Innovation Center for Advanced Materials (SICAM), Nanjing Tech University (NanjingTech), Nanjing 211816, China. E-mail: iamwhuang@njtech.edu.cn

† Electronic supplementary information (ESI) available: Synthetic procedure; experimental setup; PXRD; TG; and additional photoluminescence spectra. CCDC 1441102–1441105. For ESI and crystallographic data in CIF or other electronic format see DOI: 10.1039/c5tc04320d

exploration of **2** for highly sensitive and selective detection of Pb^{2+} and Fe^{3+} ions in aqueous solution. Although excellent studies on a highly selective fluorescent probe for the detection of Fe^{3+} were reported by Zhou's group,[10a] Sun's group,[16] and Wang's group,[13b] the advantage of **2** is that it can sense Pb^{2+} and Fe^{3+} through fluorescence enhancement and quenching, respectively. Especially, the overall quenching constant for Fe^{3+} in the concentration range of 0.02–0.1 mM is quantified to be 11 000 M^{-1}, which is comparable to that of other reports. Additionally, the luminescence behavior of **4** towards $Sm(NO_3)_3$ or $Eu(NO_3)_3$ solutions was investigated.

Experimental section

Materials and general methods

The chemicals used in this work are of analytical grade and are available commercially and were used without further purification. FT-IR spectra were recorded using KBr pellets in the range of 4000–400 cm^{-1} on a PerkinElmer FT-IR spectrometer. Elemental analyses for C, H and N were performed on a Perkin-Elmer 240C analyzer. Thermogravimetric analyses (TGA) were performed in a SHIMADZU DTG-60 simultaneous DTA-TG apparatus, under a dynamic N_2 atmosphere (20 mL min^{-1}) and a heating rate of 10 °C min^{-1} from room temperature to 800 °C. Powder X-ray diffraction investigation on the polycrystalline compounds **1–4** was carried out using a Bruker D8 advanced diffractometer equipped with a diffracted-beamed monochromator set for Cu Kα (λ = 1.5418 Å) radiation. The data were collected using a Ni-filtered Cu-target tube at room temperature in the 2θ range from 5° to 50° at an angular rate of 0.2 s per step, with a scan step width of 0.02°. Photoluminescent spectra were recorded using a PerkinElmer LS55 Fluorescence Spectrometer. Fluorescence decay curves were measured using an Edinburgh FLS920P spectrophotometer with double xenon lamp houses (one was 450 W for steady state measurements and another was 60 W microsecond flash lamp for dynamic spectrum recording).

Syntheses of $[Ln_2(FDC)_3DMA(H_2O)_3]\cdot DMA\cdot 4.5H_2O$ (1–4). A mixture of H_2FDC (0.1 mmol, 28.2 mg), $LnCl_3\cdot 6H_2O$ (0.1 mmol, Ln = Sm, Eu, Gd, Tb), imidazole (0.1 mmol), DMA (5 mL), *n*-BuOH (2 mL) and H_2O (1 mL) was sealed in a 25 mL Teflon-lined bomb and heated at 100 °C for 3 days. The reaction mixture was slowly cooled to room temperature. The colorless sheet crystals obtained were washed with ethanol and dried in air.

$[Sm_2(FDC)_3DMA(H_2O)_3]\cdot DMA\cdot 4.5H_2O$ Yield: 78%. Elemental analysis (%) calcd for $C_{118}H_{138}Sm_4N_4O_{43}$: C, 48.84; N, 1.93; H, 4.79%. Found: C, 48.66; N, 1.80; H, 4.86%. IR (KBr, cm^{-1}): 419 w, 594 w, 670 s, 790 w, 1267 vs, 1390 s, 1610 s, 2966 w, 3417 m.

$[Eu_2(FDC)_3DMA(H_2O)_3]\cdot DMA\cdot 4.5H_2O$ Yield: 80%. Elemental analysis (%) calcd for $C_{118}H_{138}Eu_4N_4O_{43}$: C, 48.73; N, 1.93; H, 4.78%. Found: C, 48.52; N, 1.85; H, 4.96%. IR (KBr, cm^{-1}): 421 w, 594 w, 673 s, 789 w, 1267 vs, 1392 s, 1610 s, 2960 w, 3515 m.

$[Gd_2(FDC)_3DMA(H_2O)_3]\cdot DMA\cdot 4.5H_2O$ Yield: 72%. Elemental analysis (%) calcd for $C_{118}H_{138}Gd_4N_4O_{43}$: C, 48.38; N, 1.91; H, 4.75%. Found: C, 48.21; N, 1.82; H, 4.87%. IR (KBr, cm^{-1}): 422 w, 597 w, 673 s, 789 w, 1267 vs, 1392 s, 1615 s, 2960 w, 3503 m.

$[Tb_2(FDC)_3DMA(H_2O)_3]\cdot DMA\cdot 4.5H_2O$ Yield: 75%. Elemental analysis (%) calcd for $C_{118}H_{138}Tb_4N_4O_{43}$: C, 48.27; N, 1.91; H, 4.74%. Found: C, 48.13; N, 1.80; H, 4.81%. IR (KBr, cm^{-1}): 418 w, 604 w, 671 s, 787 w, 1265 vs, 1396 s, 1598 s, 2960 w, 3406 m.

X-ray data collection and structure determination

The X-ray diffraction data of the single crystals of **1–4** were collected on a Bruker Smart Apex CCD area detector diffractometer using graphite-monochromated Mo-Kα radiation (λ = 0.71073 Å) at room temperature. Cell parameters were retrieved using SMART software and refined using SAINT[19] on all the observed reflections. Data were collected using a narrow-frame method with scan widths of 0.30° and an exposure time of 15 s per frame. The highly redundant data sets were reduced using SAINT and corrected for Lorentz and polarization effects. Absorption corrections were applied using SADABS[20] supplied by Bruker. Structures were solved by direct methods using the SHELX-97[21] program package. The positions of the metal atoms and their first coordination spheres were located from direct-method E maps; other non-hydrogen atoms were found using alternating difference Fourier syntheses and least-squares refinement cycles and, during the final cycles, were refined anisotropically. The suitable hydrogen atoms in the water molecules were not obtained from the difference Fourier maps and could also not be placed in calculated positions, so they were not included in the final refinement cycles. The other hydrogen atoms were placed in calculated positions and refined as riding atoms with a uniform value of Uiso. The crystallographic details for compounds **1–4** have been summarized in Table S1 (ESI†). Selected bond lengths and angles for **1–4** are listed in Tables S2–S5 (ESI†). CCDC reference numbers for **1–4** are 1441104, 1441102, 1441103 and 1441105, respectively.‡

Results and discussion

The structural features

Single-crystal X-ray diffraction revealed that compounds **1–4** are isostructural, crystallizing in triclinic space group $P\bar{1}$ (see Table S1, ESI†). Here **3** is selected as the representative example to describe the structure in detail. The asymmetric unit of **3** contains two Gd^{3+} ions, three FDC^{2-} anions, one coordinated

‡ Crystal data for **1**: triclinic, $P\bar{1}$, a = 11.4087(8) Å, b = 13.6584(8) Å, c = 24.023(1) Å, α = 93.171(4)°, β = 103.627(5)°, γ = 112.671(6)°, V = 3312.0(3) $Å^3$, Z = 1, μ(MoKα) = 1.827 mm^{-1}, ρ_{calc} = 1.455 g cm^{-3}, F(000) = 1466, GOOF = 1.225, R_1, wR_2 ($I > 2\sigma(I)$) = 0.0899, 0.2464. For **2**: triclinic, $P\bar{1}$, a = 11.4422(4) Å, b = 13.6499(5) Å, c = 23.9769(8) Å, α = 92.915(3)°, β = 103.671(3)°, γ = 112.821(3)°, V = 3311.2(2) $Å^3$, Z = 1, μ(MoKα) = 1.949 mm^{-1}, ρ_{calc} = 1.458 g cm^{-3}, F(000) = 1470, GOOF = 1.224, R_1, wR_2 ($I > 2\sigma(I)$) = 0.1089, 0.2970. For **3**: triclinic, $P\bar{1}$, a = 11.4957(4) Å, b = 13.6804(4) Å, c = 23.9693(8) Å, α = 76.328(3)°, β = 76.214(3)°, γ = 66.917(3)°, V = 3324.5(2) $Å^3$, Z = 1, μ(MoKα) = 2.049 mm^{-1}, ρ_{calc} = 1.463 g cm^{-3}, F(000) = 1474, GOOF = 1.030, R_1, wR_2 ($I > 2\sigma(I)$) = 0.0455, 0.1080. For **4**: triclinic, $P\bar{1}$, a = 11.4646(4) Å, b = 13.6288(5) Å, c = 23.7978(7) Å, α = 92.929(3)°, β = 103.548(3)°, γ = 112.494(3)°, V = 3298.6(2) $Å^3$, Z = 1, μ(MoKα) = 2.198 mm^{-1}, ρ_{calc} = 1.478 g cm^{-3}, F(000) = 1478, GOOF = 1.230, R_1, wR_2 ($I > 2\sigma(I)$) = 0.0503, 0.1269.

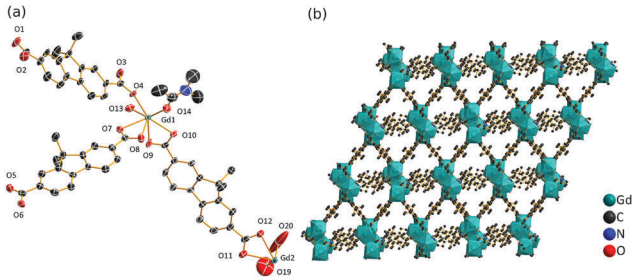

Fig. 1 View of the asymmetric unit of **3** with the thermal ellipsoids drawn at the 50% probability level (a) and the 3D framework of **3** (b). All hydrogen atoms, uncoordinated water and DMA molecules are omitted for clarity.

DMA molecule, three coordinated water molecules, one lattice DMA molecule, four and a half free water molecules (Fig. 1 and ES1†). The Gd1 ion is eight-coordinated by eight oxygen atoms: six from four different FDC^{2-} ligands, one from water molecule and one from DMA molecule. The Gd2 ion is also eight-coordinated by eight oxygen atoms: six from five different FDC^{2-} ligands and two from two water molecules. The local coordination geometries of Gd1 and Gd2 ions are bicapped trigonal prismatic geometry (Fig. S2a, ESI†). The Gd–O bond distances range from 2.302 to 2.879 Å, which are comparable to those reported for other Gd–O compounds.[22] In particular, two adjacent Gd1 ions are joined by six carboxylate groups, two of which adopt a μ_2-η_1:η_1 bridged mode to give a $[Gd_2(\mu_2\text{-}COO)_2(\mu_1\text{-}COO)_4]$ SBU with the Gd···Gd distance of 5.3263(4) Å (Fig. S2b, ESI†). Two adjacent Gd2 ions are also joined by six carboxylate groups, four of which adopt a μ_2-η_1:η_1 bridged mode to give a $[Gd_2(\mu_2\text{-}COO)_4(\mu_1\text{-}COO)_2]$ SBU with the Gd···Gd distance of 4.2658(5) Å. As shown in Fig. S2c (ESI†), the FDC^{2-} ligands act as μ_2-bridge, μ_3-bridge and μ_4-bridge, respectively. Thus, the 9,9-dimethyl-fluorene unit serves as a 2-connected linker to connect two SBUs to from a 3D neutral framework.

Thermal analysis and powder XRD

The samples were heated up to 800 °C in a N_2 atmosphere at a heating rate of 10 °C min^{-1}. The thermogravimetric (TG) curves show that **1**–**4** undergo similar weight loss processes (Fig. S3, ESI†). In the temperature range of 35–340 °C, the weight losses of **1–4** are 22.7%, 21.2%, 20.7% and 20.0%, respectively, corresponding to the departure of DMA and water molecules (calc. 21.3%, 21.3%, 21.1%, 21.1%). The PXRD patterns of **1–4** are shown in Fig. S4, ESI.† The experimental XRD patterns of the synthesized **1–4** are in good agreement with the simulated ones, showing good phase purity.

IR spectra

The presence of water in **1–4** is confirmed by the broad band in the region between 3700 and 3100 cm^{-1} characteristic of the O–H vibration (Fig. S5, ESI†). For **1–4**, bands of low intensity between 3000 and 2800 cm^{-1} show the symmetric and asymmetric C–H stretching vibrations of $-CH_3$, and the band at 1610 cm^{-1} could be assigned to the C=O vibration of DMA molecules. The typical bands in the region between 1600 and 1456 cm^{-1} are due to the C–C stretching vibrations of aromatic rings. The bands in the 1456–1320 cm^{-1} region represent the symmetric COO– stretching.

Fluorescence properties

The photoluminescence spectra of **1–4** are shown in Fig. S6 (ESI†). Upon excitation at 320 nm, the emission spectra of **1** and **3** reveal ligand-based emission centered at 368 and 372 nm, respectively. Upon excitation at 335 nm, the emission spectra of **2** reveals the characteristic emission peaks of Eu^{3+} at 592, 616, 651 and 700 nm, which are attributed to the energy transfer from the ligand to Eu^{3+} ions. Moreover **2** displays long lifetime (575 μs). Meanwhile **4** exhibits ligand-based emission centered at 362 nm and the $^5D_4 \rightarrow {}^7F_J$ (J = 6, 5, 4, and 3) characteristic transitions of Tb^{3+} ions at 478, 543, 584 and 620 nm, which can be contributed to the ineffective energy transfer from the ligand to the Tb^{3+} ion.

Metal ion sensing

The intense red luminescence of **2** promotes us to investigate its ability for sensing common metal ions. The finely ground sample of **2** was dispersed in 3 mL of 0.01 mol L^{-1} Tris-HCl solution (pH = 7.4), forming a suspension solution at a concentration of 1 mg mL^{-1} by an ultrasound method, and a solution of $M(NO_3)_x$ (40 mM) was added into the above solution to form a suspension of metal ions in water (0.2 mM). The excitation spectrum and the fluorescence decay curve are shown in Fig. S8 and S9 (ESI†), and the decrease of lifetime (293 μs) can be attributed to the interaction between water and **2**. The luminescence properties are recorded and are shown in Fig. 2. Interestingly, upon the addition of $Pb(NO_3)_2$ solution into the **2** suspension, fluorescence emission from **2** increased. Besides, Fe^{3+} exhibits a drastic quenching effect of the luminescence of **2**, while other metal ions have no significant effect on the emission with the exception of Cr^{3+} and Cu^{2+}.

The enhancing effect of Pb^{2+} is further studied using the fluorescence lifetime and titration experiments. The lifetime of $^5D_0$ in **2** increases by approximately 23.5% as the concentration

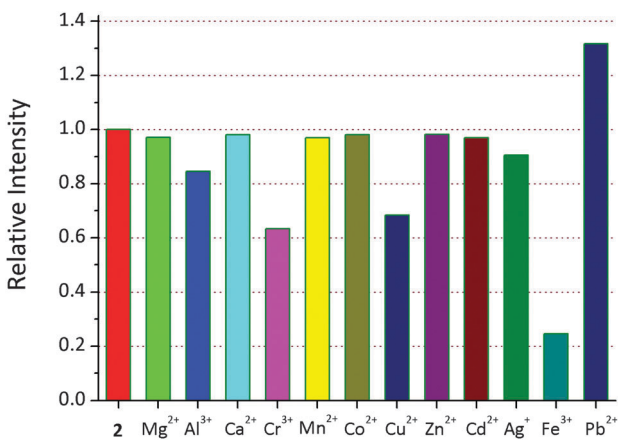

Fig. 2 Photoluminescence intensity of the $^5D_0 \rightarrow {}^7F_2$ transition (616 nm) of **2** treated with different metal ions (0.2 mM) in Tris-HCl solution.

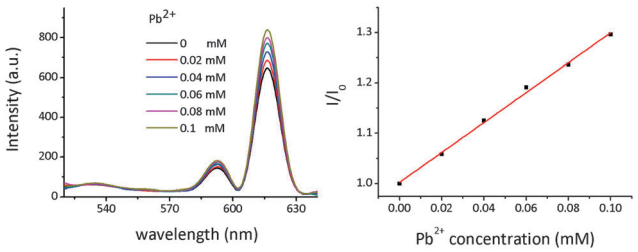

Fig. 3 Comparison of the luminescence intensity of **2** treated with different concentration of $Pb(NO_3)_2$.

of Pb^{2+} is increased from 0 to 0.1 mM (Fig. S10, ESI†). As shown in Fig. 3, the fluorescence intensity of **2** was gradually increased as the Pb^{2+} concentration increased. The relative intensity (I/I_0) had a good linear relationship with the Pb^{2+} concentration (slope = 2970 M^{-1}, R^2 = 0.997) in the concentration range of 0.02–0.1 mM, and the limit of detection of **2** for detection of Pb^{2+} ions is calculated as 8.22 μM. It is reasonable that the ligand may play a key role in the interesting fluorescence enhancement of Pb^{2+}. Although Zang' group[13a] and Wang's group[13b] had reported the fluorescence enhancement of lanthanide MOFs towards Pb^{2+} ions, **2** exhibits more excellent selectivity. Unfortunately, the mechanism of fluorescence enhancement is not clear. In the cases of Zang's report[13a] and Wang's report,[13b] disodium-2,2′-disulfonate-4,4′-oxydibenzoic acid and 3,5-di(2,4-dicarboxylphenyl)pyridine have been selected to build lanthanide MOFs, respectively. Among the three lanthanide MOFs, each one is markedly different from the others, which indicate that the possible sensing mechanism for fluorescence enhancement by the Pb^{2+} ion is a complex.

The quenching effect of Fe^{3+} was examined as a function of $Fe(NO_3)_3$ in the range of 0.1–0.5 mM. As illustrated in Fig. 4a, the fluorescence intensity is almost completely quenched at the Fe^{3+} concentration of 0.5 mM. The Stern–Volmer equation, $I_0/I = K_{SV}c + 1$ (I_0 is the initial intensity, I is the intensity at the corresponding concentration of c, and the K_{SV} is the quenching constant), was used to work out the corresponding quenching coefficient. As illustrated in Fig. 4b, it is clear that the *S–V* curve deviates from the straight line, similar to the reports of most MOF-based fluorescent sensors for Fe^{3+}.[13,16] This phenomenon suggests that both dynamic quenching and static quenching mechanisms appear in the process.

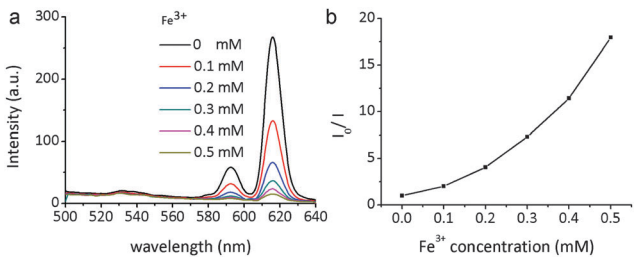

Fig. 4 Comparison of the luminescence intensity of **2** treated with different concentration of $Fe(NO_3)_3$.

Inspired by the reported MOFs for luminescence sensing of Ln^{3+},[23] the luminescence behaviors of **4** towards Sm^{3+} and Eu^{3+} ions were investigated. The finely ground sample of **4** was dispersed in 3 mL of 0.01 mol L^{-1} Tris-HCl solution, forming a suspension solution using an ultrasound method, and a solution of $Sm(NO_3)_3$ or $Eu(NO_3)_3$ (400 μM) was added into the above solution to form a suspension of metal ions in water. The luminescence properties are recorded and shown in Fig. S13–S15 (ESI†). Interestingly, upon the addition of $Eu(NO_3)_3$ solution into the **4** suspension, the emission peaks observed at 490 and 545 nm decreased gradually, while two new emission peaks at 592 and 616 nm originate from characteristic emissions of Eu^{3+} $^5D_0 \rightarrow {}^7F_J$ (J = 1, and 2) were clearly observed. Meanwhile, Sm^{3+} exhibits a distinct quenching effect on the luminescence of **4**. It is clearly that the emissions of Eu^{3+} are attributed to the energy transfer from **4** to Eu^{3+}, while the mechanism for the quenching effect of Sm^{3+} is not so clear. Thus, **4** might be a potential luminescent probe for the detection of Eu^{3+}.

The possible mechanism of fluorescence quenching

In the case of both dynamic and static quenching incorporated in the quenching process, the overall S–V curve could be

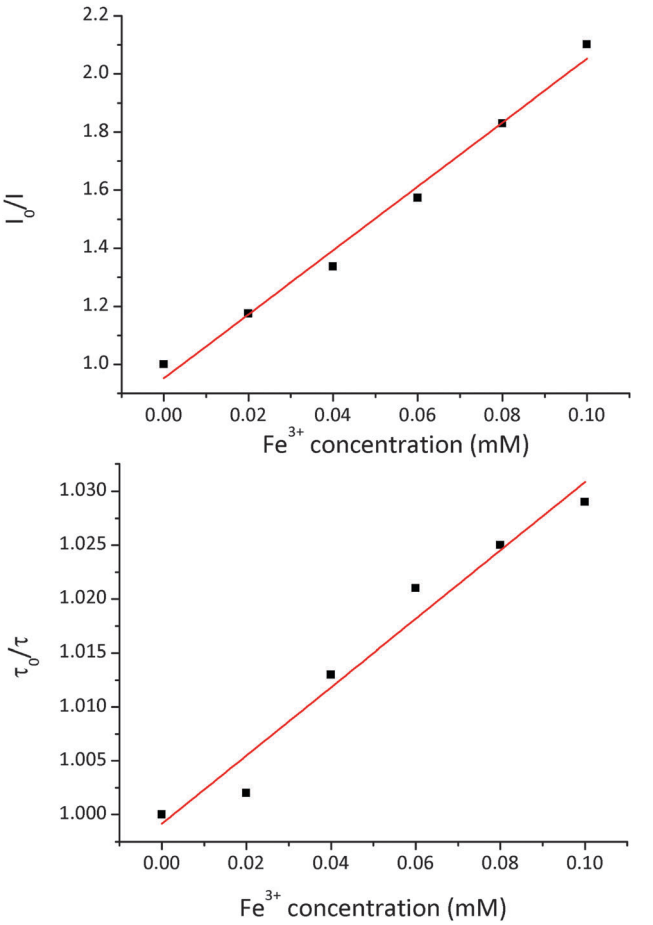

Fig. 5 The overall K_{sv} (up) and dynamic quenching constants (down) are calculated as 11 000 M^{-1} and 320 M^{-1}.

modified as $(I_0/I) = (K_D c + 1)(K_S c + 1)$, where K_D and K_S represent the dynamic quenching constant and the static quenching constant, respectively. The dynamic quenching reduces the fluorescence lifetime of **2**, while the static quenching does not. In the range of low Fe^{3+} ion concentration, $K_D K_S c^2$ could be neglected and the overall S–V equation could be simplified as a linear equation $(I_0/I) = (K_S + K_D)c + 1$. Meanwhile the dynamic quenching constant K_D can be calculated by the Stern–Volmer equation of $\tau_0/\tau = 1 + K_D c$ (τ_0 = the original lifetime of LMOF, τ = the lifetime at the analyte concentration of (c), then K_D and K_S can be obtained). Then the quenching constant of Fe^{3+} is further studied by fluorescence lifetime (Fig. S12, ESI†) and titration experiments. As illustrated in Fig. 5, the Stern–Volmer plot had a good linear relationship with the Fe^{3+} concentration (R^2 = 0.997) in the concentration range of 0.02–0.1 mM, the overall K_{SV} constant is calculated as 11 000 M^{-1}, and the limit of detection of **2** for the detection of Fe^{3+} ions is calculated as 2.22 μM. Meanwhile the lifetime S–V plot can be curve-fitted into τ_0/τ = 320 M^{-1} $[Fe^{3+}]$ + 0.999, very close to the Stern–Volmer equation. On the basis of the experimental data, the static quenching constant is calculated to be 10 680 M^{-1}. As far as we know, this K_{sv} is comparable to those in well-designed functional lanthanide MOFs for sensing Fe^{3+} ions.[13b,16]

Conclusions

In summary, we have reported a series of isostructural fluorene-based luminescent MOFs **1–4**, in which **2** is a highly selective and sensitive fluorescent sensor towards Pb^{2+} and Fe^{3+} ions. We found that I/I_0 increased linearly with Pb^{2+} concentration in the range of 0.02–0.1 mM, and the slope is 2970 M^{-1}. The dynamic and static quenching constants of Fe^{3+} in the range of 0.02–0.1 mM are 320 and 10 680 M^{-1}, which is comparable to that of the previously reported MOF Fe^{3+} sensors. And **4** displays different emissions in the presence of Sm^{3+} and Eu^{3+}. This work demonstrates the potential application of a fluorene-based EuMOF as a multiresponsive probe for the detection of Pb^{2+} and Fe^{3+} ions in the aqueous media. This present results may provide a new platform to design luminescent MOFs with applications in metal ion sensors. Further efforts will be made to synthesize functional MOFs with higher selectivity and sensitivity for Pb^{2+} and Fe^{3+}.

Acknowledgements

This work was supported by the National Natural Science Foundation of China (no. 61136003 and 51173081), the Ministry of Education of China (IRT1148), the Natural Science Foundation of Jiangsu Province (BM2012010), the Priority Academic Program Development of Jiangsu Higher Education Institutions (PAPD) (YX03001), the Specialized Research Fund for the Doctoral Program of Higher Education (SRFDP) (20113223110005), the National Basic Research Program of China (973 Program) (2012CB933301), the National Science Foundation of Jiangsu Province (BK20151512).

Notes and references

1 (*a*) B. F. Hoskins and R. Robson, *J. Am. Chem. Soc.*, 1989, **111**, 5962; (*b*) B. F. Hoskins and R. Robson, *J. Am. Chem. Soc.*, 1990, **112**, 1546.

2 (*a*) G. Ferey, *Chem. Soc. Rev.*, 2008, **37**, 191; (*b*) J. R. Long and O. M. Yaghi, *Chem. Soc. Rev.*, 2009, **38**, 1213; (*c*) L. J. Murray, M. Dincă and J. R. Long, *Chem. Soc. Rev.*, 2009, **38**, 1294; (*d*) C. Janiak and J. K. Vieth, *New J. Chem.*, 2010, **34**, 2366.

3 (*a*) O. M. Yaghi, H. Li, C. Davis, T. Richardson and T. L. Groy, *Acc. Chem. Res.*, 1998, **31**, 474; (*b*) S. Kitagawa and M. Kondo, *Bull. Chem. Soc. Jpn.*, 1998, **71**, 1739; (*c*) H. Le, M. Eddaoudi, M. O'Keefe and O. M. Yaghi, *Nature*, 1999, **402**, 276; (*d*) G. Ferey, *Chem. Mater.*, 2001, **13**, 3084; (*e*) S. Kitagawa and K. Uemura, *Chem. Soc. Rev.*, 2005, **34**, 109; (*f*) A. K. Cheetham and C. N. R. Rao, *Science*, 2007, **318**, 58.

4 (*a*) X. Wang, L. Zhang, J. Yang, F. Liu, F. Dai, R. Wang and D. Sun, *J. Mater. Chem. A*, 2015, **3**, 12777; (*b*) X. Y. Xu and B. Yan, *ACS Appl. Mater. Interfaces*, 2015, **7**, 721; (*c*) D. K. Singha and P. Mahata, *Inorg. Chem.*, 2015, **54**, 6373; (*d*) A. Li, L. Li, Z. Lin, L. Song, Z. H. Wang, Q. Chen, T. Yang, X. H. Zhou, H. P. Xiao and X. J. Yin, *New J. Chem.*, 2015, **39**, 2289.

5 L. Cui, J. Wu, J. Li and H. Ju, *Anal. Chem.*, 2015, **87**, 10635.

6 Z. Hu, K. Tan, W. P. Lustig, H. Wang, Y. Zhao, C. Zheng, D. Banerjee, T. J. Emge, Y. J. Chabal and J. Li, *Chem. Sci.*, 2014, **5**, 4873.

7 Z. Dou, J. Yu, Y. Cui, Y. Yang, Z. Wang, D. Yang and G. Qian, *J. Am. Chem. Soc.*, 2014, **136**, 5527.

8 N. B. Shustova, A. F. Cozzolino, S. Reineke, M. Baldo and M. Dincă, *J. Am. Chem. Soc.*, 2013, **135**, 13326.

9 Y. Cui, R. Song, J. Yu, M. Liu, Z. Wang, C. Wu, Y. Yang, Z. Wang, B. Chen and G. Qian, *Adv. Mater.*, 2015, **27**, 1420.

10 (*a*) X. H. Zhou, H. H. Li, H. P. Xiao, L. Li, Q. Zhao, T. Yang, J. L. Zuo and W. Huang, *Dalton Trans.*, 2013, **42**, 5718; (*b*) X. H. Zhou, L. Li, H. H. Li, A. Li, T. Yang and W. Huang, *Dalton Trans.*, 2013, **42**, 12403; (*c*) J. N. Hao and B. Yan, *J. Mater. Chem. A*, 2014, **2**, 18018.

11 (*a*) B. Liu, L. Hou, W. P. Wu, A. N. Dou and Y. Y. Wang, *Dalton Trans.*, 2015, **44**, 4423; (*b*) J. N. Hao and B. Yan, *Chem. Commun.*, 2015, **51**, 7737.

12 (*a*) W. Wang, J. Yang, R. Wang, L. Zhang, J. Yu and D. Sun, *Cryst. Growth Des.*, 2015, **15**, 2589; (*b*) S. Dang, T. Wang, F. Yi, Q. Liu, W. Yang and Z. M. Sun, *Chem. – Asian J.*, 2015, **10**, 1703; (*c*) F. Y. Yi, J. P. Li, D. Wu and Z. M. Sun, *Chemistry*, 2015, **21**, 11475.

13 (*a*) X. Y. Dong, R. Wang, J. Z. Wang, S. Q. Zang and T. C. W. Mak, *J. Mater. Chem. A*, 2015, **3**, 641; (*b*) Y.-T. Liang, G. P. Yang, B. Liu, Y. T. Yan, Z. P. Xi and Y. Y. Wang, *Dalton Trans.*, 2015, **44**, 13325.

14 (*a*) L. Liu, X. N. Zhang, Z. B. Han, M. L. Gao, X. M. Cao and S. M. Wang, *J. Mater. Chem. A*, 2015, **3**, 14157; (*b*) L. H. Cao, F. Shi, W. M. Zhang, S. Q. Zang and T. C. W. Mak, *Chemistry*, 2015, **21**, 15705; (*c*) L. N. Zhang, A. L. Liu, Y. X. Liu, J. X. Shen, C. X. Du and H. W. Hou, *Inorg. Chem. Commun.*,

2015, **56**, 137; (*d*) R. B. Lin, F. Li, S. Y. Liu, X. L. Qi, J. P. Zhang and X. M. Chen, *Angew. Chem., Int. Ed.*, 2013, **52**, 13429.
15 M. G. Campbell, S. F. Liu, T. M. Swager and M. Dincă, *J. Am. Chem. Soc.*, 2015, **137**, 13780.
16 Z. Chen, Y. Sun, L. Zhang, D. Sun, F. Liu, Q. Meng, R. Wang and D. Sun, *Chem. Commun.*, 2013, **49**, 11557.
17 Y. Gao, X. Zhang, W. Sun and Z. Liu, *Dalton Trans.*, 2015, **44**, 1845.
18 H. Tan, B. Liu and Y. Chen, *ACS Nano*, 2012, **6**, 10505.
19 *SAINT-Plus, version, 6.02, Bruker analytical X-ray System*, Madison, WI, 1996.
20 G. M. Sheldrick, *SADABSs An empirical absorption correction program, Bruker Analytical X-ray Systems*, Madison, WI, 1996.
21 G. M. Sheldrick, *Acta Crystallogr., Sect. A: Found. Crystallogr.*, 2008, **64**, 112.
22 X. P. Yang, R. A. Jones, J. H. Rivers and R. P. Lai, *Dalton Trans.*, 2007, 3936.
23 J. S. Qin, S. J. Bao, P. Li, W. Xie, D. Y. Du, L. Zhao, Y. Q. Lan and Z. M. Su, *Chem. – Asian J.*, 2014, **9**, 749.